Articles in PresS. Am J Physiol Heart Circ Physiol (July 21, 2006). doi:10.1152/ajpheart.00571.2006

Title

Role of Diastolic Properties in the Transition to Failure in a Mouse Model of Cardiac Dilatation

Authors
[1]Peter N. Costandi
[2]Lawrence R. Frank
[1]Andrew D. McCulloch
[1]Jeffrey H. Omens

Affiliation
[1]Department of Bioengineering, University of California, San Diego, La Jolla, California, 92093-0613, USA
[2]Department of Radiology, University of California, San Diego, La Jolla, California, 92093-0613, USA

Running Head
Diastolic Properties and the Transition to Heart Failure

Contact Information
Peter N. Costandi
Department of Bioengineering
University of California, San Diego
La Jolla, CA 92093-0613 USA
pcostand@ucsd.edu
Phone: (858)534-3631
Fax: (858)534-0522

Copyright Information

Copyright © 2006 by the American Physiological Society.

ABSTRACT

Although the physiological states of hypertrophic remodeling and congestive heart failure have been intensively studied, less is known about the transition from one to the other. The use of genetically engineered murine models of heart failure has proven valuable in characterizing the progression of remodeling and its ultimate decompensation to failure. Mice deficient in the cytoskeletal muscle LIM-only protein are known to present with a clinical picture of dilated cardiomyopathy and transition to failure as adults. Longitudinal high field MR cardiac imaging provided a time course of remodeling where an improvement in ejection fraction and stroke volume (15wk vs. 31wk $MLP^{(-/-)}$: $P<0.0001$) was temporally concurrent with an abrupt phase of end-diastolic chamber dilatation. Hemodynamic analysis conducted throughout that dilatation phase showed improved dP/dt_{max}/EDP (15wk vs. 31wk $MLP^{(-/-)}$: $P<0.0005$), dP/dt_{min}/EDP (15wk vs. 31wk $MLP^{(-/-)}$: $P<0.003$) and developed pressure (15wk vs. 31wk $MLP^{(-/-)}$: $P<0.0001$) levels in the $MLP^{(-/-)}$. Computational modeling techniques were used to estimate the end diastolic pressure volume relationship revealing that, although MLP hearts possess a stiffer stress-strain relation, chamber compliance increased as a function of dilatation. This detailed physiological characterization during a phase of rapid anatomical remodeling suggests that systolic function in the $MLP^{(-/-)}$ may temporarily improve as a result of alterations in chamber compliance, which are mediated by dilatation. In turn, a balance may exist between exploiting the Frank Starling mechanism and altering chamber compliance that maintains function in the absence of hypertrophic growth. Though initially compensatory, this process may exhaust itself and consequently transition to a maladaptive course.

Keywords:
Heart failure, magnetic resonance imaging, dilatation, finite element modeling, diastolic properties

Copyright Information

INTRODUCTION

The discrete, physiological states of hypertrophic remodeling (30) (19) and congestive heart failure (13) have been well studied. The dynamic nature of the heart allows it the plasticity to progressively change structurally to accommodate an inciting stimulus in an attempt to maintain parameters, such as myocardial mass and cardiac output, to within physiological ranges (3). This compensatory remodeling has a limit, beyond which congestive heart failure may ensue (20).

Although the individual stages of hypertrophy and heart failure have been extensively studied, the transition from one to the other has not been fully characterized. The factors that influence the inability to further compensate and give way to overt failure remain unclear. The objectives of this study were to quantify the time course of anatomical and functional changes that occur during the transition towards overt failure and to investigate the role of dilatation in altering passive mechanics during that period. A mechanism is then proposed that describes how these dilatation-mediated changes in chamber compliance may maintain function in the absence of hypertrophic growth. A combination of imaging, surgical hemodynamic analysis, and computational modeling methods was employed to allow the assessment of longitudinal changes in global cardiac structure and function in the mouse.

Genetically engineered murine models have become valuable tools in the study of heart failure by providing populations of a similar and reproducible phenotype (31). In particular, the targeted deletion of cytoskeletal proteins, such as the muscle LIM-only protein (MLP), have been shown to consistently lead to dilated cardiomyopathy and heart failure in mice (2) (17). Echocardiography and *in vivo* pressure-volume loop measurements performed on failing adult MLP deficient mice ($MLP^{(-/-)}$) have revealed many of the clinical characteristics associated with congestive heart failure (7). Recent work has investigated whether diastolic function, including passive mechanics, is altered in the $MLP^{(-/-)}$ model (26) (20). Omens et al have shown alterations in the passive pressure-volume and pressure-strain relations, concluding a less compliant tissue in the adult dilated hearts versus age matched controls (27). Lorenzen-Schmidt et al have found notable alterations in passive myocardial properties and relaxation times in young $MLP^{(-/-)}$ mice, which present with a more compliant tissue at 2 weeks but normal characteristics for most systolic parameters (21). Though these results suggest the progression to heart failure in this model may be a consequence of diastolic dysfunction, a driving mechanism that mediates these changes has yet to be revealed. The hypothesis of the present study was thus that the relative effects of diastolic left ventricular properties, in particular those due to dilatation and material stiffness, mediate chamber compliance and thus may influence systolic function.

Clearly, $MLP^{(-/-)}$ mice progress through a distinct evolution in both morphology and function from an early age of virtually normal systolic performance to overt failure. However, little is known about that transition or the stimuli that lead to these changes. In this study, the novel application of longitudinal magnetic resonance (MR) imaging in conjunction with invasive catheter techniques was used to investigate the time course of remodeling in this clinically relevant heart failure model. Finite element analysis, integrating data from both techniques, was used to estimate the end diastolic pressure volume relationship and describe the relative balance between factors determining its

Copyright Information

shape. Results have revealed a distinct transitional period where dilatation is temporally concurrent with an increase in systolic function. The balance between diastolic properties that shifts in favor of dilatation may increase chamber compliance, initially maintaining or improving function, but eventually decompensating as overt heart failure ensues.

Copyright Information

MATERIALS and METHODS

Mouse Model

MLP-deficient mice (2) used in this study were obtained from a University of California, San Diego (UCSD) colony. Homozygous $MLP^{(-/-)}$ mice were inbred so that wildtype littermates were not available. The background strain to the $MLP^{(-/-)}$ was a hybrid cross of 129/Sv and C57BL/6 strains. After 20 generations of intercrossing, genetic marker analysis showed an indistinguishable background between the $MLP^{(-/-)}$ and 129/Sv genotypes, making age-matched 129/Sv mice (Charles River) an appropriate wildtype control (unpublished data). All protocols were performed according to the National Institutes of Health *Guide for the Care and Use of Laboratory Animals* and approved by the UCSD Animal Subjects Committee.

MRI Study

Animal Preparation and Monitoring

Eight mice {four $MLP^{(-/-)}$ (2 male, 2 female) and four 129/Sv (2 male, 2 female)} were imaged longitudinally at a weekly interval from 2-3 to 32 weeks of age with no mortality. Anesthesia was chamber induced with 5 Vol-% inhaled isoflurane in 100% O_2, then sustained under free breathing conditions in a custom built restraint with 1.5 Vol-% isoflurane at 1.5l/min for the remainder of the imaging session. External copper foil or subcutaneous needle ECG leads were placed on the front forelimbs for ECG triggering (HSB-T, Rapid Biomedical) while a rectal thermocouple probe monitored core body temperature held constant by heated airflow through the magnet bore. Mice were maintained and observed at 450-550 BPM and 36-38°C using a custom designed physiological monitoring system integrated with a data acquisition network (LabVIEW 6.1, National Instruments).

MR Imaging

In vivo NMR cardiac imaging was performed on a 7T horizontal-bore MR scanner (Varian, Palo Alto, CA), equipped with a shielded 12cm bore gradient system capable of 22G/cm gradient strength and a 300μs maximum rise time (Magnex Scientific, Oxford, UK). A 1.9cm custom built dual quadrature driven transverse electromagnetic mode (TEM) volume coil was used for transmission and reception of the RF signal.

High resolution bright blood MRI experiments were conducted using an ECG triggered Fast Low Angle SHot (FLASH) Gradient Echo (GE) pulse sequence tailored for murine imaging as previously described (8). Scanning parameters optimized for signal to noise were found to be: flip angle=90°, echo time=1.8ms, repetition time~R-R interval (~120ms), receiver bandwidth=32kHz, and number of averages=5. Fractional echo (62.5%) to reduce the echo time and time series averaging were employed, both of which serve to increase the signal to noise ratio. A field of view of $25mm^2$ and data matrix of 128^2 was prescribed to yield an in-plane resolution of $195\mu m^2$.

Each imaging protocol resulted in 7-9 1mm thick short axis images spanning the whole heart from apex to base. A prospective gating scheme was used where images were acquired at a range of time delays relative to the ECG trigger in temporal increments of 10ms. Equatorial frames containing the largest and smallest chamber diameters were selected as the diastolic and systolic phases of the cardiac cycle, respectively.

Copyright Information

Image Analysis

Four two-dimensional contours were manually planimetered for each heart at end-diastole and end-systole (LV (and RV) epi and endo) using an image analysis software (ImageJ, NIH). From calibrated units, contour areas were calculated, multiplied by the slice thickness, and summed together to approximate volumes. LV mass was obtained by subtracting endocardial from epicardial volumes and scaling by the specific gravity of myocardial tissue (1.055 g/ml). Stroke volume was defined as LVEDV-LVESV while ejection fraction was calculated as 100 x SV/LVEDV.

Control Studies

A validation study was conducted at 36 weeks using two 129/Sv controls and two $MLP^{(-/-)}$ to assess the accuracy of MR mass ($MR_{mass,mg}$) measurement versus wet weight ($WW_{mass,mg}$), which served as the standard. Immediately following imaging, mice were euthanized, the hearts harvested, and weighed for comparison. Linear regression analysis showed good correlation between MR and gravimetry [$MR_{mass,mg} = WW_{mass,mg}(1.02) - 4.99$] where the offset is a measure of the volume artifact associated with blood flow within the ventricle during the time between phase encoding and readout. Oblique flow artifacts can cause artifactual displacement of flow intensities that can overlap the endocardial wall, resulting in a slight overestimation of the cavity volume (10) (9). These effects were minimized by the use of short echo times.

Hemodynamic and Tissue Analysis

Eighty seven mice {forty one $MLP^{(-/-)}$ (29 males, 12 females) and forty six 129/Sv (24 males, 22 females)} were used in terminal studies at four time points: 8, 15, 22, and 31 weeks of age. All eighty seven yielded body, heart, lung and liver weight data at the time of euthanasia. Forty eight mice (eight of each strain at each of three time points: 15, 22, 31) underwent hemodynamic analysis.

Millar Conductance Catheter Experiment

Continuous and simultaneous pressure and volume measurements were invasively obtained directly from the left ventricular cavity by a procedure described elsewhere (25). Briefly, mice were induced with 5 Vol-% inhaled isoflurane and maintained via nosecone at 2 Vol-% while warmed by a circulating water blanket (K Module, American Pharmaseal Co.). A midline cervical incision exposed the trachea for intubation with a cannula connected to a volume cycled rodent ventilator (Model 687, Harvard Apparatus, Inc.). The right carotid artery was exposed and isolated via the same incision. A 1.4F Mikro-Tip conductance catheter (SPR-839, Millar Instruments) was introduced into the carotid artery, advanced down the ascending aorta, through the aortic valve and into the left ventricle. Pressure and volume measurements were recorded under steady state conditions.

Hemodynamic data was analyzed using software designed for conductance catheter measurements (PVAN3.3, Millar Instruments). Volume data was calibrated and corrected for parallel conductance by hypertonic saline injection as previously described (33). Relative volume units were calibrated to microliters using heparinized blood in cuvettes of a known volume (910-1049, Millar Instruments). All hemodynamic data was averaged over 10 beats for each animal.

Finite Element Modeling

Copyright Information

The chamber compliance of a heart may be influenced by two factors that are related by a highly non-linear relationship: the stiffness of the myocardium, as reflected in the stress-strain relationship, and the geometry of the ventricle. For modeling purposes geometry was described with wall thickness and radius measurements. Computational methods make it possible to assess the relative contribution of these two components on passive mechanics separately. To that end, computational finite element techniques were used to estimate the end diastolic pressure volume relationship (EDPVR) in each of fourteen mice (seven $MLP^{(-/-)}$ and seven 129/Sv) before (week 15) and after (week 31) the dilatation phase using software developed in our lab (Continuity 6.3, www.continuity.ucsd.edu). MR imaging provided geometric data for modeling at end-diastole while the hemodynamic analysis supplied pressure and volume data throughout the cardiac cycle. Wall thickness and radius measurements from the MR images yielded wall and cavity volumes at the end-diastolic state, from which volumes of a smaller chamber radius may be extrapolated by unloading the model with pressure while maintaining conservation of mass. A least squares optimization routine was used to fit two variables, the V_0 (unloaded) geometry and a single material constant within the constitutive law, to two points known to lie along the EDPVR, the end-diastolic pressure/volume point and the volume at minimum pressure point.

Finite Element Model

The complex cardiac geometry required approximation by an analytical geometrical model. A truncated prolate spheroidal geometry was used to model the LV of the heart, where the inner and outer radii of the mesh at the equatorial plane were set to the measured values from MR image analysis. A high-order {Linear(λ, transmural)-Cubic(μ, longitudinal)-Cubic(θ, circumferential)} three element mesh was used. Similar meshes have previously been shown to give converged solutions as compared with a low-order 70 element mesh (4). Both element and numerical convergence were confirmed by mesh refinement to a 288 element mesh and evaluation of inflation volume to within 3% error. Apical nodes were constrained in λ with respect to the longitudinal element coordinate, apical and basal nodes were constrained in μ with respect to the transmural element coordinate, while the mesh was constrained from rigid body motion and rotation as previously described (4).

Passive Mechanical Properties

Stress and strain in the LV were modeled with a transversely isotropic exponential strain energy function (Eq. 1), with respect to the fiber coordinate system (fiber, cross-fiber, sheet), that has previously been used to describe resting myocardium (15).

$$W = \tfrac{1}{2}C(e^{Q} - 1) + C_{\text{compr}}\{I_3 (\ln I_3) - I_3 + 1\} \qquad \text{Eq. 1}$$

$$Q = b_{\text{ff}}E^2_{\text{ff}} + b_{\text{xx}}(E^2_{\text{cc}} + E^2_{\text{ss}} + E^2_{\text{cs}} + E^2_{\text{sc}}) + b_{\text{fx}}(E^2_{\text{fc}} + E^2_{\text{cf}} + E^2_{\text{fs}} + E^2_{\text{sf}})$$

The constitutive law contains five material constants (C, C_{compr}, b_{ff}, b_{xx}, b_{fx}) that must be fit to strain measurements (E^2_{ij}). The material constant to be estimated was the stress-scaling coefficient (C), which linearly scales the strain energy function (W), and hence the inflation pressure. The remaining four parameters were fixed at values derived from a fit to normal rat myocardium: {bulk modulus (C_{compr}) = 100.0 kPa, fiber strain exponent

Copyright Information

(b_{ff}) = 9.2, transverse strain exponent (b_{xx}) = 2.0, fiber-transverse shear exponent (b_{fx}) = 3.7} (26). The tangential slope of the EDPVR is then directly proportional to the magnitude of *C*. A larger value for *C*, therefore, indicates a stiffer curve. By varying one constant in the constitutive law it is possible to fit the EDPVR to two hemodynamic points and estimate the desired two unknowns (V_0 and *C*). A passive inflation was modeled for each heart using its unique V_0 geometry and constitutive relation at 2.5mmHg increments to compute the EDPVR.

Statistical Analysis

All data are expressed as means ± S.E.M. Statistical comparisons were made by two-way Analysis of Variance followed by Fisher's PLSD post-hoc analysis over time and genotype. Statistical differences of $P < 0.05$ were considered significant.

Copyright Information

RESULTS

Weights

Body and tissue weights measured during the terminal hemodynamic analysis are summarized in Table 1. Although body weights of $MLP^{(-/-)}$ mice did not differ from wildtype controls, heart, liver and lung weights per tibial length were increased significantly at each time point ($P<0.0007$). The wet/dry heart weight ratio between strains was also not significant, indicating that the increase in $MLP^{(-/-)}$ heart mass is due to hypertrophy and not edema.

MRI

A weekly imaging protocol resulted in 142 MRI experiments. For clarity, data is presented in Figures 1 and 2 at 18 time points, where the mean of all mice imaged at the nearest three time points, i.e. 2-4 wks, 5-7 wks, etc., ± S.E.M. is shown for each genotype.

The time course for a dilatation index, defined as the ratio of LV chamber volume to LV epicardial volume (chamber plus myocardial volume) at end-diastole, which serves as a three-dimensional analog of a radius to wall thickness ratio, is illustrated in Figure 1(a). As the chamber radius increases relative to the epicardial surface volume, the index will approach unity, indicating dilatation. In $MLP^{(-/-)}$ hearts the epicardial volumes smoothly plateau (data not shown), whereas the endocardial volumes experienced an increase (15wk vs. 24wk $MLP^{(-/-)}$: $P<0.0001$), as shown in Figure 1(b), leading to an elevated dilatation index among strains ($MLP^{(-/-)}$ vs. 129/Sv: $P<0.01$). Of particular note was the abrupt increase in this index. Prior to about 18 weeks of age, $MLP^{(-/-)}$ hearts had geometrical ratios comparable to wildtypes, but progressed through a rapid phase of dilatation in the following 8-9 weeks to plateau again near week 27 (15wk vs. 24wk $MLP^{(-/-)}$: $P<0.0001$). This accelerated rate of remodeling was reproducible throughout the sample group and marks a clear transition in ventricular geometry.

Though the dilatation index in the $MLP^{(-/-)}$ remained comparable to controls through week 15, hypertrophic growth in the LV was observed far earlier, as is reflected by myocardial mass shown in Figure 2. LV mass peaks and plateaus near week 15 in both strains ($MLP^{(-/-)}$ vs. 129/Sv: $P<0.05$), indicating the cessation of hypertrophic growth. Although the mean decreased in the $MLP^{(-/-)}$ from 15 to 31 weeks, no statistical difference was found in heart weight (data not shown) or heart weight/tibial length (Table 1).

By comparing diastolic MR images with those acquired at end-systole, functional information may be derived. The time courses of ejection fraction and stroke volume are described in Figures 1(c) and 1(d). The $MLP^{(-/-)}$ hearts presented with a normal ejection fraction (EF) at two weeks of age as compared to wildtypes but quickly declined into failure ($MLP^{(-/-)}$ vs. 129/Sv: $P<0.05$), as reflected in what is most likely edematous lung and liver tissue (Table 1). Although this relative depression persisted throughout the study, ejection fraction improved in the $MLP^{(-/-)}$ with a pattern temporally concurrent with dilatation (15wk vs. 24wk $MLP^{(-/-)}$: $P<0.005$), as can be seen when the curves are compared on a common time axis. Though the mean in 129/Sv stroke volume and ejection fraction varied with time post maturity (~8 wks), significance between any two time points was only found between the highest and lowest values measured.

Hemodynamic Analysis

Copyright Information

The longitudinal MR study revealed a distinct phase of rapid end-diastolic dilatation beginning around week 18 and continuing through about week 27 that was accompanied by an apparent intragroup improvement in systolic performance. These trends were also used to define periods of significant change when more invasive and quantitative hemodynamic analysis was conducted. Three such times were chosen to precede (week 15), coincide with (week 22) and follow (week 31) the dilatation phase. The hemodynamic study supplemented the end-diastole and end-systole volume measurements from MR with pressure and volume data throughout the cardiac cycle. No statistical difference was found in heart rate between time points or among strains. Representative pressure/volume (P-V) loop data from 22 week $MLP^{(-/-)}$ and 129/Sv hearts are shown in Figure 3. Note the dilated ventricle and depressed systolic pressure in the $MLP^{(-/-)}$. A number of indices extracted from the P-V data are summarized in Figure 4. It was again seen that ejection fraction (15wk vs. 31wk $MLP^{(-/-)}$: $P<0.0001$) and stroke volume (15wk vs. 31wk $MLP^{(-/-)}$: $P<0.0001$) in the $MLP^{(-/-)}$ increase through the dilatation phase (Fig. 4a and 4b), corroborating results of the MR longitudinal study. Additionally, parameters based on pressure measurements were calculated. At week 15 the end-diastolic pressure (EDP) in the $MLP^{(-/-)}$ was elevated ($MLP^{(-/-)}$ vs. 129/Sv: $P<0.0001$) (Fig. 4c), but approached control levels at weeks 22 ($MLP^{(-/-)}$ vs. 129/Sv: $P=0.19$) and 31 ($MLP^{(-/-)}$ vs. 129/Sv: $P=0.47$). Within the knockout strain EDP continued to fall from week 15 to 31 (15wk vs. 31wk $MLP^{(-/-)}$: $P=0.0002$). End-systolic pressure in the $MLP^{(-/-)}$ was significantly depressed versus control ($MLP^{(-/-)}$ vs. 129/Sv: $P<0.0001$), with little significant change from 15 to 31 weeks in either strain ($P=0.03$) (data not shown). The ability of $MLP^{(-/-)}$ hearts to generate pressure from an end-diastolic state (maximum – minimum pressure, Fig. 4d) was depressed compared with wildtype ($MLP^{(-/-)}$ vs. 129/Sv: $P<0.0001$), but increased from 15 to 31 weeks in the $MLP^{(-/-)}$ (15wk vs. 31wk $MLP^{(-/-)}$: $P<0.0001$). Load independent velocities of both contraction (15wk vs. 31wk $MLP^{(-/-)}$: $P<0.0005$) and relaxation (15wk vs. 31wk $MLP^{(-/-)}$: $P<0.003$) were both improved in the $MLP^{(-/-)}$ during the same period, recovering from levels depressed versus wildtype at week 15 ($MLP^{(-/-)}$ vs. 129/Sv: $P<0.0001$) to those comparable at week 31 ($MLP^{(-/-)}$ vs. 129/Sv: $P>0.13$) (Fig. 4e and 4f). Furthermore, these improving trends are temporally concurrent with the phase of rapid dilatation. The time courses of volume related parameters from the catheter experiments were consistent with the results of the MRI study. Also, there was good agreement in the statistically significant differences found between strains at corresponding time points where both techniques were used.

EDPVR Modeling

The key results from the finite element (FE) models are summarized in Table 2, including the calculated values for V_0 and C. Of note is the accuracy with which the FE model estimated the end-diastolic volume when inflated to the EDP as compared to direct ventricular measurement. The unloaded volumes in 15 week $MLP^{(-/-)}$ hearts were comparable to wildtype, but increased significantly at 31 weeks (15wk vs. 31wk $MLP^{(-/-)}$: $P=0.0002$) (31 wk $MLP^{(-/-)}$ vs. 129/Sv: $P<0.0001$), most likely as a function of chamber dilatation. These results are in accord with the end-diastolic volumes measured from longitudinal MR imaging. Myocardial stiffness was seen to increase significantly, both from 15 to 31 weeks in the $MLP^{(-/-)}$ (15wk vs. 31wk $MLP^{(-/-)}$: $P<0.05$) and between strains at both time points (15 wk $MLP^{(-/-)}$ vs. 129/Sv: $P<0.05$) (31 wk $MLP^{(-/-)}$ vs. 129/Sv: $P=0.0002$). This agrees with previous results that show older $MLP^{(-/-)}$ hearts to

Copyright Information

have a stiffer stress-strain relationship (27). The simulated passive inflation of each heart with its unique V_0 and constitutive law is illustrated in Figure 5. Although having a stiffer myocardium, there was little difference in chamber compliance between strains at week 15. In contrast, compliance increased markedly in the 31 week $MLP^{(-/-)}$ despite further myocardial stiffening. This demonstrates the concept that myocardial stiffness can increase, but chamber stiffness can decrease due to the impact of chamber dilatation.

Copyright Information

DISCUSSION

The $MLP^{(-/-)}$ model is known to consistently develop a phenotypic picture of clinical dilated cardiomyopathy with systolic dysfunction (right shifted P-V loops, depressed systolic contractility, increased LV ED and ES dimensions, decreased percent fractional shortening) and transition to overt heart failure as an adult (20-28 wks), although at two weeks of age mice appear to have systolic function comparable to wildtype controls (7) (21). However, the time course of that progression or its governing factors remains unknown. The aim of this study was thus to characterize this evolution and examine the role of myocardial stiffness and ventricular dilatation in altering chamber compliance and mediating systolic function.

Results of this study have uncovered an abrupt dilatation phase beginning around week 18 and continuing through week 27 in the $MLP^{(-/-)}$. Although depressed versus control, ejection fraction, stroke volume, developed pressure, dP/dt_{max}/EDP and dP/dt_{min}/EDP were all found to increase temporally concurrent with this dilatory phase. Thus there appears to be a compensatory phase during the progression toward heart failure in this model in which systolic function may actually transiently improve in the dilated ventricle.

Computational modeling showed that, despite increasing myocardial stiffness over time, dilatation led to a more compliant ventricle in the 31 week $MLP^{(-/-)}$ compared with wildtype or younger knockouts. These results suggest a shifting balance between the effects of geometry and material properties on chamber compliance. At week 15, the slightly stiffer curve may be a function of the increased myocardial stiffness, as reflected in the elevated stress-scaling coefficient, and the lack of any dilatation, resulting in a decreased chamber compliance in $MLP^{(-/-)}$. As the ventricle dilates yet continues to stiffen, the balance shifts in favor of geometrical change resulting in a heart with increased compliance.

The factors that impact the nonlinear relationship between diastolic pressure and volume have been well documented. Glantz et al have proposed a mathematical model that illustrates the balance between ventricular geometry and material stiffness on chamber compliance (14). They incorporate geometry in a wall thickness to radius ratio, η, and show that, for a given material stiffness, increasing the ratio shifts the P-V curves leftward while decreasing it has the opposite effect. Mirsky et al echo the importance of geometry on diastolic behavior by including a wall to chamber volume ratio as an analog to η (22). In the canine, Laks et al have shown hypertrophy shifts P-V curves leftward (18) while Gaasch et al have shown dilatation in human hearts move flattened curves toward higher pressures (11). Increasing wall stiffness while holding geometry constant in the Glantz model shifts P-V curves leftward. Smith et al demonstrate the same effect in man following myocardial infarction before dilatation dominates the balance (29). We propose that the balance in this dichotomy plays a prominent role in remodeling and the progression towards overt failure in the $MLP^{(-/-)}$.

The striated muscle specific protein MLP is expressed at high levels in atrial and ventricular myocytes during development and in the adult (1). It is believed that MLP is an essential promoter of proper cardiomyocyte architectural organization within the heart wall, where genetically engineered models lacking this protein present with significant disruption in ultrastructure (2). In addition, MLP has been proposed to play an important

Copyright Information

role in mechanotransduction and the control of hypertrophic remodeling via the titin/Tcap/MLP/α-actinin complex (17). In the present study, at around 15 weeks hypertrophic growth appears to diminish for unclear reasons. The hypertrophic stimulus may have been removed, or is still present but the heart is no longer able to properly sense the load, possibly due to the mechanotransduction deficiency associated with the gene deletion. Although tissue mass has peaked by week 15, anatomical and functional changes continue through week 31, suggesting they are not directly related to hypertrophic growth. The temporary improvement in systolic performance during that time is thus likely attributable to other adaptations that are not sustainable as the mice age and transition to failure. It is well known that stroke volume improves with an increased LV cavity size, as may be the case during eccentric hypertrophy and normal physiologic growth (5). Dilatation may thus serve as a mechanical pathway to augment stroke volume during this particular phase. However, without an increase in percent wall thickening, dilatation, even with the accompanying increased stroke volume, will result in a decreased ejection fraction that will eventually result in the failure that has classically been associated with a dilating ventricle (6) (28). In the event that both stroke volume and ejection fraction increase with dilatation, one may propose that systolic function must also increase. This premise is supported by measures of dP/dt/EDP and developed pressure. The basis for this improvement may lie in the changes in chamber compliance, which are mediated by dilatation.

A mechanism by which these changes in compliance attempt to maintain systolic performance during this period remains undefined. Subsequent to week 15, remodeling no longer seems to be driven by hypertrophic growth, but rather may be governed by dilatation, and the associated alterations in passive mechanics. At week 15 the EDPVR in the $MLP^{(-/-)}$ is comparable to controls. At that time, EDP is elevated suggesting that, in the continued absence of geometrical change via dilatation, function is being maintained by the Frank-Starling mechanism where working pressures are higher up on the EDPVR curve. As the pressures continue to rise, a physiological limit may be reached where stiffness becomes extremely high and there is little change in volume for a given change in pressure. A phase of dilatation may ensue to serve multiple purposes. First, chamber compliance of the ventricle will increase, aiding in filling. Second, working pressures will decrease back towards normal levels restoring the ability to again operate on increasing portions of the Frank-Starling curve. These two effects may manifest in the improved or maintained stroke volume and ejection fraction observed during the dilatory phase. These results also suggest that there may be multiple mechanisms of growth and recovery and that change may progress in a cyclical fashion, where the balance in contribution may shift between these preferred pathways depending on the condition of the heart at that time. In the $MLP^{(-/-)}$, function may initially be maintained by the Frank-Starling mechanism, but subsequently by anatomical restructuring as stiffness increases in the absence of hypertrophic growth This balance is mediated by changes in chamber compliance, which are in turn mediated by dilatation. A limit to this compensatory mechanism may be reached that marks the threshold to overt failure.

Non-invasive high field cardiac MR imaging has proven to be a powerful tool in assessing both anatomy and function in the mouse model (23). In order to characterize transitional phases within a process, it is essential to non-invasively monitor changes in the same animal as they develop. In this longitudinal study, MR techniques were applied

Copyright Information

to obtain a high resolution time course of left ventricular remodeling that spanned an 8 month time frame from about 2 to 32 weeks of age. The dilatory phase revealed is typically thought of as an event marking a transition towards overt heart failure. In this model there appeared to be a transient remodeling phase in which dilatation is associated with enhanced systolic function. The motivation thus existed to further characterize the hemodynamic state of the $MLP^{(-/-)}$ heart at various time points throughout this period. Pressure and volume data taken directly from the LV via catheter insertion provided a detailed hemodynamic picture to supplement the findings of the MR study. Ejection fraction and stroke volume were again found to increase during dilatation, in agreement with MR measurements. Finite element analysis provided a platform for the integration of both experimental techniques in estimating the end diastolic pressure volume relationship before and after the dilatation phase. By fitting the curve to hemodynamic data, this approach made it possible to assess the effects of geometry and material properties separately. Such time courses may also be valuable in defining targeted time points where the up/down regulation of genes may modulate the hypertrophic response.

There are several possible sources of error associated with each experimental technique as well as the mouse model. Although the MR images have sufficient spatial resolution in plane, longitudinal resolution was limited to a 1mm slice thickness, affecting volume calculations. Also, the volume effects associated with bright blood imaging may impact endocardial delineation. The summed effect of both was estimated to be on the order of 3-5% by linear regression to wet weight. Catheter studies are suspected of having sources of error attributed predominantly to the nonlinear electrical properties of the myocardium. The underestimation of absolute volumes as compared to MR is a documented deficiency with conductance catheters in the mouse (16). Moreover, volumes are often a function of calibration, contributing to the discrepancy between MR and hemodynamic values, yet relative changes between time points and among strains are not. Care was taken to consistently calibrate the volume measurements, making statistically significant differences in time valid. Volume traces are also particularly sensitive to catheter orientation within the ventricle. Despite its limitations, conductance catheters have been successfully applied to murine cardiac studies (25) (33) (24). Both MR and catheter techniques demonstrate the same temporal trends in volume related indices, lending further credibility to the results presented here. A potential limitation to finite element modeling was the reduction of an exponential constitutive law to a single scaling variable. With only one degree of freedom, it was not necessary that the EDPVR would pass through the two hemodynamic points. Although convergence would improve with more degrees of freedom, least squares optimization for the data presented was within 2% error. The estimated value of C was also relatively insensitive to V_0, which was derived from physiological measurements. Linear regression for the 31 week $MLP^{(-/-)}$ group, for example, was $C = V_0(0.11) - 1.8$ with $R^2 = 0.98$. The FE models could be improved with more detailed geometries, such as non-axisymmetric models, and with improved constitutive laws that allow for anisotropic materials accounting for laminar sheet structure. With respect to the animal model, $MLP^{(-/-)}$ mice are certainly undergoing normal growth in addition to pathological hypertrophy during development. This study focuses on a time period where heart mass has stabilized (HW: 1.8%, BW: 0.7% change from 15-31wks), minimizing the confounding factors that any growth may play. Anatomically, mice are at the extreme of

Copyright Information

the thickness to radius and thickness to myocyte diameter ratio (32). They also differ kinematically and metabolically (12), mainly due to the accelerated heart rate. Despite these limitations, mouse models are crucial for understanding human myocardial growth and remodeling.

In summary, the remodeling process in a genetically engineered mouse model of heart failure has been characterized in detail during a phase of major anatomical and functional change. Multiple experimental techniques were integrated to reveal a transitional period that has not been previously described. Systolic parameters such as ejection fraction, stroke volume, developed pressure, dP/dt_{max}/EDP and dP/dt_{min}/EDP all improve temporally concurrent with this phase of rapid end-diastolic dilatation. These finding support the proposition that this improvement may be the result of alterations in chamber compliance, which are mediated by dilatation. In turn, a balance may exist between exploiting the Frank Starling mechanism and altering chamber compliance that maintains function in the absence of hypertrophic growth. Though initially compensatory, this process will eventually exhaust itself and consequently transition to a maladaptive course.

Copyright Information

AKNOWLEDGEMENTS

This work was supported by the National Institutes of Health (grants HL64321, HL46345, and HL107444), the National Biomedical Computation Resource (NIH grant P41 RR08605), and the National Science Foundation (grant BES-0506252). We thankfully acknowledge Dr. Masahiko Hoshijima for providing the $MLP^{(-/-)}$ mice and Dr. James Covell for his insightful discussions.

Copyright Information

REFERENCES

1. **Arber S, Halder G, and Caroni P.** Muscle LIM Protein, a Novel Essential Regulator of Myogenesis, Promotes Myogenic Differentiation. *Cell* 79: 221-231, 1994.
2. **Arber S, Hunter J, Ross J, Hongo M, Sansig G, Borg J, Perriard J, and Chien K.** MLP-Deficient Mice Exhibit a Disruption of Cardiac Cytoarchitectural Organization, Dilated Cardiomyopathy, and Heart Failure. *Cell* 88: 393-403, 1997.
3. **Bishop S.** Ultrastructure of the Myocardium in Physiologic and Pathologic Hypertrophy in Experimental Animals. *Perspectives in Cardiovascular Research* 7: 127-147, 1983.
4. **Costa K, Hunter P, Wayne J, Waldman L, Guccione J, and McCulloch A.** A Three-Dimensional Finite Element Method for Large Elastic Deformations of Ventricular Myocardium: II--Prolate Spheroidal Coordinates. *Journal of Biomechanical Engineering* 11: 464-472, 1996.
5. **Emery J and Omens J.** Mechanical Regulation of Myocardial Growth During Volume Overload Hypertrophy in the Rat. *American Journal of Physiology Heart Circulation Physiology* 42: H1198-H1204, 1997.
6. **Ertl G, Gaudron P, Eilles C, and Kochsiek K.** Serial Changes in Left Ventricular Size After Acute Myocardial Infarction. *American Journal of Cardiology* 68: 116D-120D, 1991.
7. **Esposito G, Santana L, Dilly K, Cruz J, Mao L, Lederer O, and Rockman H.** Cellular and Functional Defects in a Mouse Model of Heart Failure. *American Journal of Physiology Heart Circulation Physiology* 279: H3101-H3112, 2000.
8. **Frahm J, Haase A, and Matthaei D.** Rapid NMR Imaging of Dynamic Processes Using the FLASH Technique. *Magnetic Resonance in Medicine* 3: 321-327, 1986.
9. **Frank L and Buxton R.** Distortions From Curved Flow in Magnetic Resonance Imaging. *Magnetic Resonance in Medicine* 29: 84-93, 1993.
10. **Frank L, Crawley A, and Buxton R.** Elimination of Oblique Flow Artifacts in Magnetic Resonance Imaging. *Magnetic Resonance in Medicine* 25: 299-307, 1992.
11. **Gaasch W, Cole J, Quinones M, and Alexander J.** Dynamic Determinants of Left Ventricular Diastolic Pressure-Volume Relations in Man. *Circulation* 51: 317-323, 1975.
12. **Gibbs C.** Cardiac Energetics: Sense and Nonsense. *Clinical and Experimental Pharmacology & Physiology* 30(8): 598-603, 2003.
13. **Gillebert T, Leite-Moreira A, and Hert S.** Load Dependent Diastolic Dysfunction in Heart Failure. *Heart Failure Reviews* 5: 345-355, 2000.
14. **Glantz S and Parmley W.** Factors Which Affect the Diastolic Pressure-Volume Curve. *Circulation Research* 42: 171-180, 1978.
15. **Guccione J, McCulloch A, and Waldman L.** Passive Material Properties of Intact Ventricular Myocardium Determined From a Cylindrical Model. *Journal of Biomechanical Engineering* 113: 42-55, 1991.
16. **Jacoby C, Molojavyi A, Flogel U, Merx M, Ding Z, and Schrader J.** Direct Comparison of Magnetic Resonance Imaging and Conductance Microcatheter in the Evaluation of Left Ventricular Function in Mice. *Basic Research in Cardiology* 101: 87-95, 2006.

Copyright Information

17. **Knoll R, Hoshijima M, Hoffman H, Person V, Lorenzen-Schmidt I, Bang M, Hayashi T, Shiga N, Yasukawa H, Schaper W, McKenna W, Yokoyama M, Schork N, Omens J, McCulloch A, Kimura A, Gregorio C, Poller W, Schaper J, Schultheiss H, and Chien K.** The Cardiac Mechanical Stretch Sensor Machinery Involves a Z Disc Complex that Is Defective in a Subset of Human Dilated Cardiomyopathy. *Cell* 111: 943-955, 2002.
18. **Laks M, Morady F, Garner D, and Swan H.** Relation of Ventricular Volume, Compliance, and Mass in the Normal and Pulmonary Arterial Banded Canine Heart. *Cardiovascular Research* 6: 187-198, 1972.
19. **Lin H, Katele K, and Grimm A.** Functional Morphology of the Pressure- and the Volume Hypertrophied Rat Heart. *Circulation Research* 41: 830-836, 1977.
20. **Lorell B.** Transition From Hypertrophy to Failure. *Circulation* 96: 3824-3827, 1997.
21. **Lorenzen-Schmidt I, Stuyvers B, Ter Keurs H, Date M, Hoshijima M, Chien K, McCulloch A, and Omens J.** Young MLP Deficient Mice Show Diastolic Dysfunction Before the Onset of Dilated Cardiomyopathy. *Journal of Molecular Cell Cardiology* 39: 241-250, 2005.
22. **Mirsky I and Parmley W.** Assessment of Passive Elastic Stiffness of Isolated Heart Muscle and the Intact Heart. *Circulation Research* 33: 233-243, 1973.
23. **Nahrendorf M, Hiller K, Hu K, Ertl G, Haase A, and Bauer W.** Cardiac Magnetic Resonance Imaging in Small Animal Models of Human Heart Failure. *Medical Image Analysis* 7: 369-375, 2003.
24. **Nemoto S, Defreitas G, Mann D, and Carabello B.** Effects of changes in left ventricular contractility on indexes of contractility in mice. *American Journal of Physiology Heart Circulation Physiology* 283: H2504-H2510, 2002.
25. **Nishio R, Sasayama S, and A M.** Left Ventricular Pressure-Volume Relationship in a Murine Model of Congestive Heart Failure Due to Acute Viral Myocarditis. *Journal of American Collage of Cardiology* 40: 1506-1514, 2002.
26. **Omens J, MacKenna D, and McCulloch A.** Measurement of Strain and Analysis of Stress in Resting Rat Left Ventricular Myocardium. *Journal of Biomechanics* 26: 665-676, 1993.
27. **Omens J, Usyk T, Li Z, and McCulloch A.** Muscle LIM Protein Deficiency Leads to Alterations in Passive Ventricular Mechanics. *American Journal of Physiology Heart Circulation Physiology* 282: H680-H687, 2002.
28. **Seals A, Pratt C, Mahmarian J, Tadros S, Kleiman N, Roberts R, and Verani M.** Relation of Left Ventricular Dilation During Acute Myocardial Infarction to Systolic Performance, Diastolic Dysfunction, Infarct Size and Location. *American Journal of Cardiology* 61: 224-229, 1988.
29. **Smith M, Russell R, Feild B, and Rackley C.** Left Ventricular Compliance and Abnormally Contracting Segments in Postmyocardial Infarction Patients. *Chest* 65: 368-378, 1974.
30. **Spann J.** Contractile and Pump Function of the Pressure-Overloaded Heart. *Perspectives in Cardiovascular Research* 7: 19-38, 1983.
31. **Wang Q, Bohlooly M, and PO S.** Murine Models for the Study of Congestive Heart Failure: Implications for Understanding Molecular Mechanisms and for Drug

Copyright Information

Discovery. *Journal of Pharmacological and Toxicological Methods* 50: 163-174, 2004.

32. **Wessels A and Sedmera D.** Developmental Anatomy of the Heart: a Tale of Mice and Man. *Physiological Genomics* 15(3): 165-176, 2003.
33. **Yang B, Larson D, and Watson R.** Age-Related Left Ventricular Function in the Mouse: Analysis Based on In Vivo Pressure-Volume Relationships. *American Journal of Physiology Heart Circulation Physiology* 277: H1906-H1913, 1999.

Copyright Information

FIGURE LEGENDS

Figure 1
MRI derived time courses of remodeling for MLP$^{(-/-)}$ vs 129/Sv. 142 MRI experiments from a weekly imaging protocol are summarized at 18 binned time points. Plots are presented as the mean of all mice imaged at the nearest three time points, i.e. 2-4 wks, 5-7 wks, etc., ± S.E.M. for each genotype. Note the presence of hypertrophy up to 15 weeks, as indicated by a comparable dilatation index among strains (a) but a larger EDV (b) in the MLP$^{(-/-)}$, and the abrupt dilatation phase [bracket below data in (a) and (b)] that occurs temporally concurrent with an increase in SV (c) and EF (d).
MLP$^{(-/-)}$ vs 129/Sv: ‡ $P<0.05$
15wk vs 31wk MLP$^{(-/-)}$: † $P<0.0001$

Figure 2
MRI derived time course of LV myocardial mass for MLP$^{(-/-)}$ vs 129/Sv. Plots are again presented as the binned mean of all mice imaged at the nearest three time points ± S.E.M. for each genotype. Note the presence of hypertrophic growth in the MLP$^{(-/-)}$ from an early age and its termination at around week 15. There were no statistically significant differences in body weight found between strains at any time point.
MLP$^{(-/-)}$ vs 129/Sv: ‡ $P<0.05$

Figure 3
Representative P-V Loop Data for 22 week 129/Sv vs MLP$^{(-/-)}$. Ten consecutive cardiac cycles are shown for each heart. Note the elevated chamber volumes in the MLP$^{(-/-)}$, indicative of LV dilatation, and the depression in systolic pressures.

Figure 4
Measured parameters from hemodynamic analysis for MLP$^{(-/-)}$ vs 129/Sv. 48 hemodynamic experiments are summarized. Graphs are presented as the mean ± S.E.M. for each genotype. Note the improvement in systolic function that occurs during the dilation phase. Also note the decreasing EDP.
MLP$^{(-/-)}$ vs 129/Sv: ‡‡ $P<0.0001$, ‡ $P<0.005$
15wk vs 31wk MLP$^{(-/-)}$: †† $P<0.0001$, †† $P<0.001$, † $P<0.05$

Figure 5
EDPVR modeled with finite element analysis for MLP$^{(-/-)}$ vs 129/Sv. Curves are fitted to volumes numerically estimated from finite element models at two time points for both genotypes. Shaded symbols are the two hemodynamic points used to fit each EDPVR, while open symbols are the calculated unloaded volumes (V_0). S.E.M for all modeled volumes ranged from 0.04 to 1.4µl. Note the increased chamber compliance of hearts at week 31, despite a stiffer myocardium. Also note the higher working pressures in the week 15 MLP$^{(-/-)}$ versus control, but comparable pressures in the week 31 MLP$^{(-/-)}$.

Copyright Information

Table 1
Weights of MLP$^{(-/-)}$ vs. 129/Sv at 8, 15, 22 and 31 weeks

		Body Weight (g)	Heart/TL (mg/cm)	Lung/TL (mg/cm)	Liver/TL (g/cm)	Heart Wet/Dry Weight
8 Week	129/Sv	23.21 ± 0.79	49.09 ± 1.57	64.18 ± 2.18	0.406 ± 0.012	4.009 ± 0.470
	MLP$^{(-/-)}$	21.71 ± 0.68	73.69 ± 1.99	90.74 ± 1.40	0.567 ± 0.027	4.194 ± 0.110
	P-value	NS	$P < 0.0001$	$P < 0.0001$	$P = 0.0002$	NS
15 week	129/Sv	26.93 ± 0.89	57.34 ± 2.15	70.23 ± 1.39	0.493 ± 0.023	4.833 ± 0.237
	MLP$^{(-/-)}$	29.36 ± 0.94	85.72 ± 2.32	96.69 ± 4.83	0.653 ± 0.025	4.829 ± 0.161
	P-value	NS	$P < 0.0001$	$P < 0.0001$	$P = 0.0002$	NS
22 week	129/Sv	28.52 ± 0.93	59.40 ± 2.94	76.23 ± 2.58	0.506 ± 0.017	4.901 ± 0.434
	MLP$^{(-/-)}$	30.19 ± 0.52	84.81 ± 1.42	92.27 ± 2.90	0.713 ± 0.020	5.149 ± 0.313
	P-value	NS	$P < 0.0001$	$P = 0.0005$	$P < 0.0001$	NS
31 week	129/Sv	31.30 ± 0.60	71.74 ± 3.15	79.11 ± 2.92	0.589 ± 0.026	4.710 ± 0.316
	MLP$^{(-/-)}$	29.61 ± 0.85	82.96 ± 2.15	88.88 ± 1.81	0.704 ± 0.024	5.189 ± 0.729
	P-value	NS	$P = 0.0056$	$P = 0.0066$	$P = 0.0039$	NS

Values are mean ± S.E.M.
NS = Not Significant

Copyright Information

Table 2
End-Diastolic Volume and Stiffness

	Wall Thickness (mm)	**Radius (mm)**	**FEM End Diast Vol (µl)**	**Millar End Diast Vol (µl)**	**V_0 FEM (µl)**	**Stress-Scaling Coeff. (kpas)**
15 wk 129/Sv	0.71 ± 0.03	1.96 ± 0.03	28.02 ± 0.06	27.77 ± 0.04	14.7 ± 0.75	0.74 ± 0.13
31 wk 129/Sv	0.65 ± 0.02	1.85 ± 0.04	28.03 ± 0.06	28.33 ± 0.03	14.8 ± 0.11	0.80 ± 0.02
15 wk MLP$^{(-/-)}$	0.71 ± 0.01	1.91 ± 0.04	31.81 ± 0.06	31.83 ± 2.59	16.4 ± 1.41	1.19 ± 0.07
31 wk MLP$^{(-/-)}$	0.70 ± 0.02	2.37 ± 0.09	45.16 ± 0.11	45.02 ± 1.26	29.2 ± 0.61	1.52 ± 0.08

Values are mean ± S.E.M.

Copyright Information

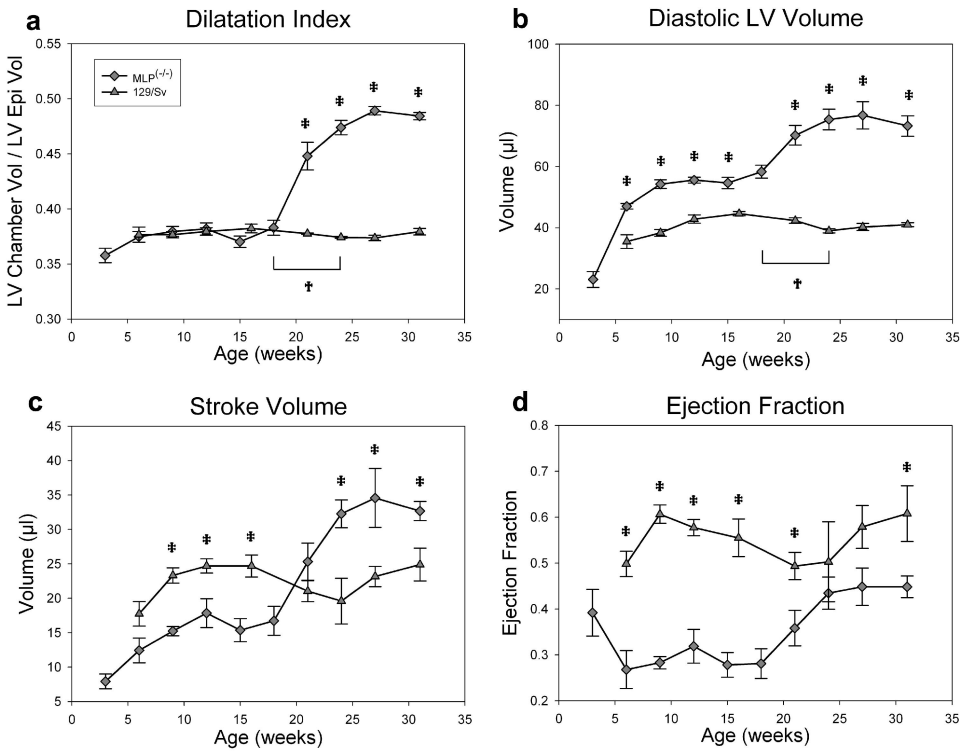

MRI derived time courses of remodeling for MLP$^{(-/-)}$ vs 129/Sv. **142 MRI experiments from a weekly imaging protocol are summarized at 18 binned time points. Plots are presented as the mean of all mice imaged at the nearest three time points, i.e. 2-4 wks, 5-7 wks, etc., ± S.E.M. for each genotype. Note the presence of hypertrophy up to 15 weeks, as indicated by a comparable dilatation index among strains (a) but a larger EDV (b) in the MLP$^{(-/-)}$, and the abrupt dilatation phase [bracket below data in (a) and (b)] that occurs temporally concurrent with an increase in SV (c) and EF (d).**

Copyright Information

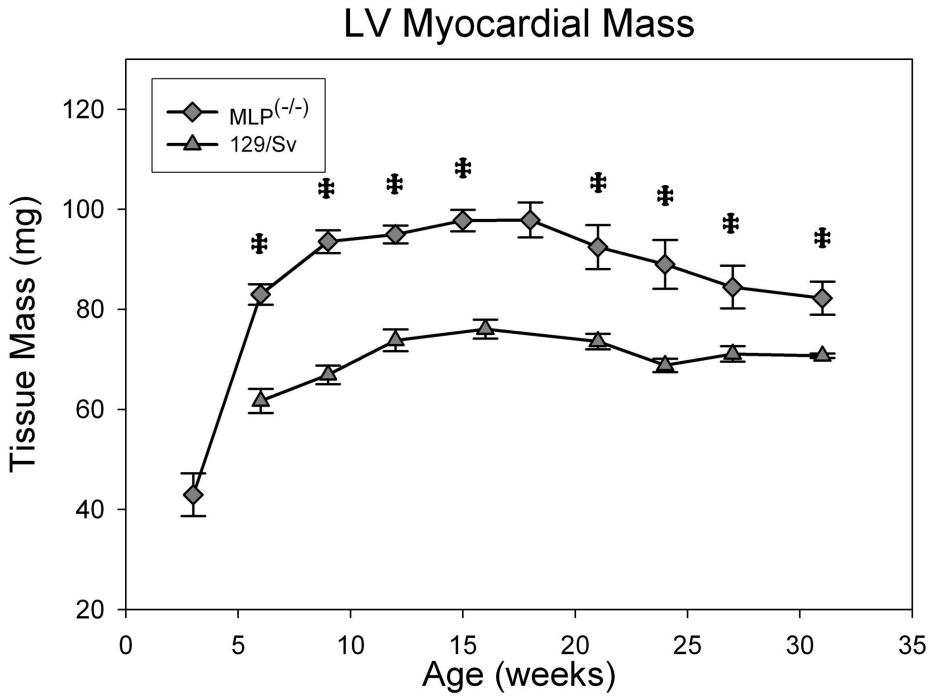

MRI derived time course of LV myocardial mass for MLP$^{(-/-)}$ vs 129/Sv. **Plots are again presented as the binned mean of all mice imaged at the nearest three time points ± S.E.M. for each genotype. Note the presence of hypertrophic growth in the MLP$^{(-/-)}$ from an early age and its termination at around week 15. There were no statistically significant differences in body weight found between strains at any time point.**

Copyright Information

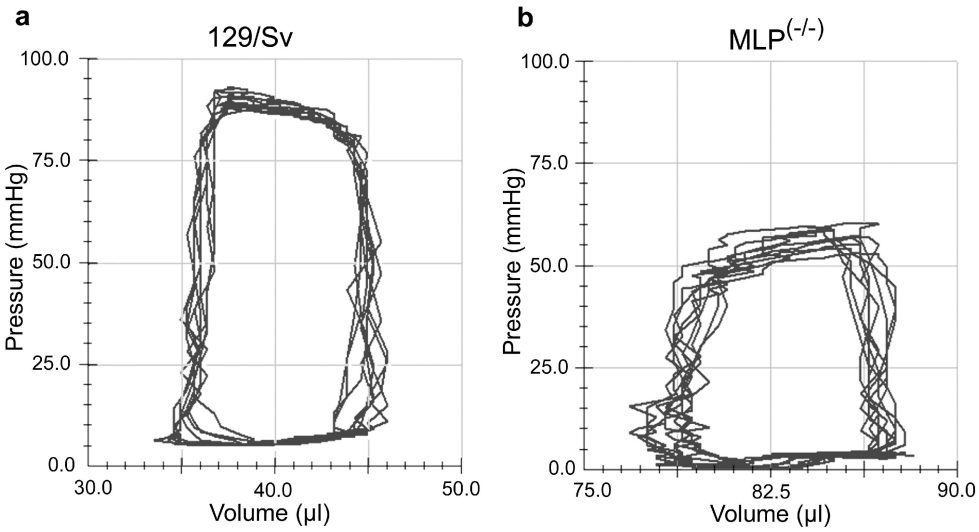

Representative P-V Loop Data for 22 week 129/Sv vs MLP$^{(-/-)}$. **Ten consecutive cardiac cycles are shown for each heart. Note the elevated chamber volumes in the MLP$^{(-/-)}$, indicative of LV dilatation, and the depression in systolic pressures.**

Copyright Information

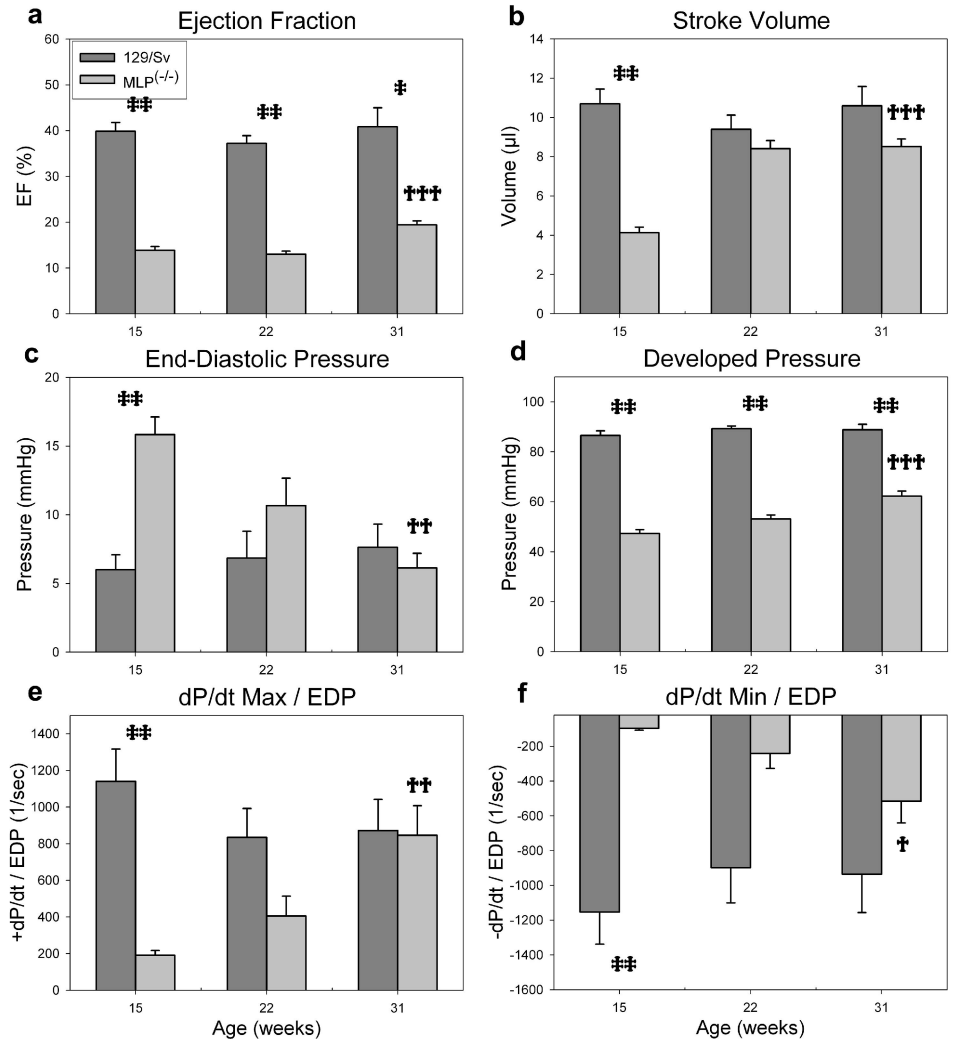

Measured parameters from hemodynamic analysis for MLP$^{(-/-)}$ vs 129/Sv. **48 hemodynamic experiments are summarized. Graphs are presented as the mean ± S.E.M. for each genotype. Note the improvement in systolic function that occurs during the dilation phase. Also note the decreasing EDP.**

Copyright Information

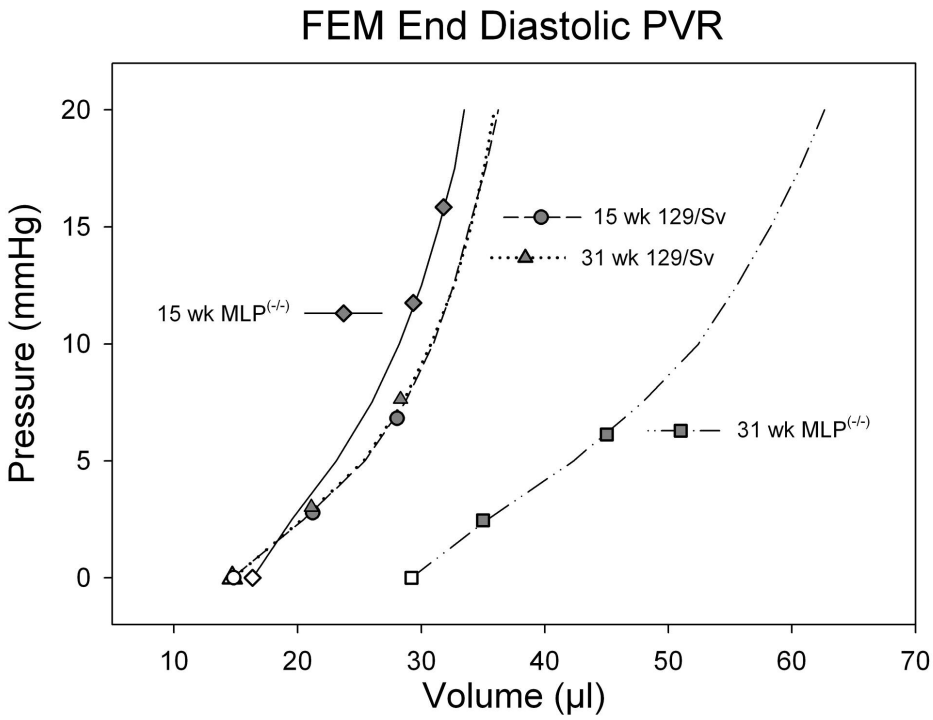

EDPVR modeled with finite element analysis for MLP$^{(-/-)}$ vs 129/Sv. **Curves are fitted to volumes numerically estimated from finite element models at two time points for both genotypes. Shaded symbols are the two hemodynamic points used to fit each EDPVR, while open symbols are the calculated unloaded volumes (V_0). S.E.M for all modeled volumes ranged from 0.04 to 1.4ul. Note the increased chamber compliance of hearts at week 31, despite a stiffer myocardium. Also note the higher working pressures in the week 15 MLP$^{(-/-)}$ versus control, but comparable pressures in the week 31 MLP$^{(-/-)}$.**

Copyright Information